Pergamon

Int. J. Heat Mass Transfer. Vol. 41, No. 10, pp. 1177–1188, 1998

Printed in Great Britain
0017–9310/98 $19.00+0.00

PII: S0017–9310(97)00222–6

Melting and resolidification of a substrate in contact with a molten metal: operational maps

S.-P. WANG,† G.-X. WANG‡ and E. F. MATTHYS§

Department of Mechanical and Environmental Engineering, University of California, Santa Barbara, CA 93106, U.S.A.

(*Received* 23 *December* 1996 *and in final form* 24 *July* 1997)

Abstract—The melting and resolidification of the substrate or of previously deposited layers may play an important role in many processes such as thermal spray coating, microcasting, spray deposition and high-temperature casting. A good understanding of this phenomenon would help us to achieve better bonding between deposited layers in some cases or to avoid damage to the substrate in others. In the present work, these processes are looked at as the melting and resolidification of a substrate in contact with a layer of molten metal which may also solidify. Both the solidification of the deposited layer and the melting and then resolidification of the substrate or previous layer are calculated using nonequilibrium phase change kinetics conditions at the solid–liquid interfaces and an implicit finite difference method with interface tracking. A nondimensional analysis of the controlling parameters under various conditions was conducted, and allowed us to generate nondimensional operational maps that can tell us whether there will be substrate melting or not. If there is, other nondimensional maps were generated to quantify the maximum achievable melting depth for various process conditions. Some results on the interface velocity during substrate melting and resolidification for various process conditions and for variations in interfacial heat transfer coefficient with time are also presented. © 1998 Elsevier Science Ltd.

1. INTRODUCTION

Whether a deposited melt may induce substrate melting or not is an important consideration in many manufacturing process involving solidification of metals. In continuous slab or strip casting processes, substrate melting may be detrimental because of wheel or mold damage, for example. In contrast, in other processes involving deposition of multiple layers of material, good bonding between successive layers or between layer and substrate may be essential. This would be the case for spray deposition, microcasting, coating and similar processes involving the deposition of metal droplets on a substrate or previously deposited layer. For example, in addition to mechanical attachment of the coating layer on the substrate due to the micro-roughness of the latter, a strong bonding between the coating and the substrate can also be formed by the metallurgical interactions at the interface between the sprayed coating and the substrate through substrate melting [1–5]. For instance, such a metallurgical interaction was observed between molybdenum and a steel substrate sprayed in the flame wire process [1]. Harmsworth and Stevens [6] have also observed a thin interfacial amorphous film existing at the interface between a plasma sprayed zirconia coating and a pre-deposited bond layer. The formation of this amorphous thin layer is believed to result from a fusion between the two layers due to the partial melting and rapid quenching of the outer surface of the bond layer.

Another interesting process relying on remelting is microcasting [4, 5, 7], which involves the deposition of successive droplets of metal to build-up parts. For low-melting temperature materials, a high superheat of the incoming droplet must be achieved in order to remelt the previous layers deposited. The superheat should, however, be controlled to achieve appropriate melting of the substrate in order to ensure adequate metallurgical bonding and therefore part integrity, yet should not be unnecessarily high. The interface interaction between the two layers is a complex phenomenon, and is affected by the physical properties of the materials used and by the thermal state of the layers in contact. A good understanding of this substrate melting phenomenon after melt deposition is, therefore, essential to achieve good control of the interface bonding between the layers.

Although process designers have long relied on melting of the substrate during thermal spray deposition, and although various numerical models have also been developed to simulate the melt spreading and solidification, see for example [8–12], relatively little analysis on the substrate remelting phenomenon has been performed. Kuijpers and Zaat [13] conducted an approximate analytical analysis of the heat transfer in both deposit and substrate by assuming two semi-infinite bodies in perfect contact. This analy-

† Visiting Scientist from the Department of Engineering Mechanics, Tsinghua University, Beijing 100084, China.

‡ Presently with the Center for Thermal Spray Research, SUNY, Stony Brook, NY, U.S.A.

§ Author to whom correspondence should be addressed.

NOMENCLATURE

b	deposit thickness [m]
Bi	$=hb/\lambda_{L1}$
C_P	specific heat [J kg-K^{-1}]
d	substrate molten depth [m]
d_{max}	maximum substrate melting depth [m]
h	heat transfer coefficient between deposit and substrate
L	latent heat of solidification [J kg^{-1}]
q_s	heat flux in or out of the deposit top surface [W m^{-2}]
Q_s	$=q_s b/[\lambda_{L1}(T_{M2}-T_0)]$ dimensionless heat flux
Ste	$=C_L(T_{M2}-T_0)/L_1$ Stefan number
T	temperature [K]
T_0	substrate initial temperature [K]
T_M	equilibrium melting temperature [K]
T_P	pouring temperature [K]
ΔT_P	melt superheat upon impact [K]
t	time [s]
V_i	S–L interface velocity [m s^{-1}]
y	spatial coordinate perpendicular to the substrate–deposit interface [m]
y_{LS}	S–L interface location [m]
Y	nondimensional elevation.

Greek symbols

α	thermal diffusivity [m^2 s^{-1}]
ε	nondimensional S–L interface elevation
η	nondimensional computational coordinate in the solid phase
λ	thermal conductivity [W m-K^{-1}]
μ_k	linear kinetics coefficient [m s-K^{-1}]
ρ	density [kg m^{-3}]
θ	$=(T-T_0)/(T_{M2}-T_0)$ dimensionless temperature
θ_{Pc}	minimum θ_P leading to substrate melting
τ	nondimensional time
ξ	nondimensional computational coordinate in the liquid phase.

Subscripts

c	critical condition at which the substrate starts melting
i	at the S–L interface
j	solid or liquid phase
L	liquid
P	at pouring conditions
S	solid
M	equilibrium melting temperature
N	nucleation temperature
O	at the deposit–substrate interface
1	deposit
2	substrate.

Superscripts

i	at the S–L interface
A	before substrate melting
B	after substrate melting.

sis can give an interface temperature between the splat and the substrate. If this temperature is higher than the melting temperature of the substrate, they concluded that the substrate would melt. Later, Zaat [2] used the same technique to calculate the minimum particle temperature needed to heat the substrate to its melting temperature. More recently, Steffens *et al.* [3] used this approach again to explain the interface bonding mechanism of thermally sprayed metal and ceramic composites on metallic substrates. Their tensile strength measurements of the coatings indicated that a higher interface temperature above the substrate melting temperature would usually lead to a better bonding between the coating and the substrate. Although this type of thermal analysis provides some qualitative insight into the interfacial heat transfer condition in spray deposition, it does not provide much quantitative information. In addition, many assumptions are needed to obtain an analytical formulation for the interface temperature, e.g. no melt superheat upon impact, no melt undercooling during solidification, and perfect contact between the coating and the substrate; and the actual melting of the substrate is not included.

Clearly, solving this type of problem analytically requires many simplifications, which leads one to investigate numerical analysis instead. The first numerical model that analyzes the melting of the substrate appears to have been developed by Amon *et al.* [4, 5] for a highly superheated molten metal droplet impinging on various substrates in the microcasting process. Some important quantitative information such as the critical conditions for the substrate melting, the melting front location, etc., are indeed provided by their model. The model assumed, however, perfect contact between the metal layer and the substrate. Sobolev *et al.* [14] have developed a numerical model to study the substrate-coating thermal interaction during high velocity of oxyfuel spraying of WC-12Co on a steel substrate. The thermal contact resistance between the coating and the substrate was also introduced into the model. The modeling results were used to determine the optimal conditions of the substrate and coating structure formation in the

process. A similar model has also been developed by Kang *et al.* [15] to investigate the melting of a tin droplet impacting on a substrate, and later impacted itself by a second droplet.

In our work, we have performed a systematic investigation of the substrate melting and resolidification problem when a molten layer is deposited and rapidly solidified on the substrate. This generic problem could be looked at as a splat impacting on a substrate or a previous splat, or just as readily as a layer of metal in contact with a mold (we call these 'deposit' on 'substrate' hereafter for simplicity). Both the deposit solidification and the melting and resolidification of the substrate are modeled. Two main objectives were aimed at: (1) the development of more comprehensive models including for example the nonequilibrium phase change kinetics at the interfaces that may be important during rapid solidification or melting, and also the variation with time of the interfacial thermal contact between deposit and substrate; and especially (2) the generation of generic information on these processes that might be readily useful to process designers.

2. PHYSICAL MODEL, MATHEMATICAL FORMULATION AND NUMERICAL SOLUTION

2.1. *Model and governing equations*

Looking at the droplet deposition process, for example, the droplet impact and spreading is completed over a time scale much shorter than the time needed for the droplet to solidify if the droplet is sufficiently large [4, 5, 9–11]. The initial spreading process can, therefore, be justifiably neglected in this case in order to simplify the analysis. Because the splat thickness is also usually much smaller than its diameter, a one-dimensional heat conduction analysis of both the splat and the substrate is generally appropriate. In other processes such as continuous casting of thin slab or strip, the geometry may also lend itself to this simplification. Pure materials with a distinct phase change temperature are considered here for both deposit and substrate, but with provisions made to allow interface temperature deviations from the equilibrium which are treated by introducing linear kinetics of phase change. A heat transfer coefficient is also introduced at the interface between the deposit and the substrate to quantify the thermal resistance due to a nonperfect contact between the two surfaces. The value of this interfacial heat transfer coefficient will likely vary significantly during the process when the surface conditions change [16], and such variations are incorporated in the model.

Using these assumptions, the problem can be treated as a one-dimensional heat conduction problem with (possibly nonequilibrium) phase change taking place at two solid/liquid fronts, one in the deposit and the other in the substrate (Fig. 1). The basic governing equation is

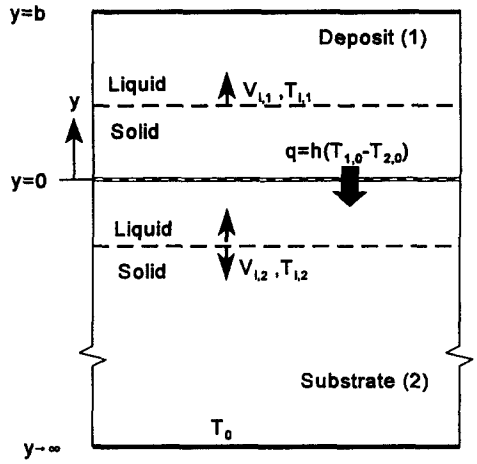

Fig. 1. Schematic of the modeling geometry.

$$\rho_j C_{Pj} \frac{\partial T_j}{\partial t} = \frac{\partial}{\partial y}\left(\lambda_j \frac{\partial T_j}{\partial y}\right) \tag{1}$$

where the subscript j stands for either solid (S) or liquid (L) phase in either deposit (1) or substrate (2).

The thermal contact resistance between the deposit and the substrate is quantified by a heat transfer coefficient h corresponding to a boundary condition at this interface, written as

$$+\lambda_j \frac{\partial T_j}{\partial y}\bigg|_{y=0} = h(T_{1,0} - T_{2,0}) \tag{2}$$

where $T_{1,0}$ and $T_{2,0}$ are the temperatures of the deposit and of the substrate at $y = 0$. It should be pointed out that the thermal contact resistance is a complex function of the processing conditions and the process configuration, and only very limited quantitative data are available for a few processes. However, a compilation of values for the interfacial heat transfer coefficient, h for several rapid solidification processes including droplet splat cooling, strip casting and melt spinning was recently published by some of the authors [17], and provides quantitative information about this coefficient.

Some other boundary and initial conditions are also needed. The substrate temperature far away from the deposit is assumed in this case to remain at the initial substrate temperature T_0:

$$T_2[y = -\infty, t] = T_0. \tag{3}$$

The top surface of the deposit can be subject to a heat flux, q_s which can be either into (negative) or out of (positive) the deposit:

$$-\lambda_1 \frac{\partial T_1}{\partial y}\bigg|_{y=b} = q_s \tag{4}$$

where b is the deposit thickness. For example, heat could be transferred from the hot plasma gas into the deposit during plasma thermal spraying, but heat could also be transferred out during splat cooling and

melt-spinning due to radiation or convection between the deposit and the environment.

The deposit and substrate are assumed to be initially at uniform temperatures equal to the 'pouring' and to the 'ambient' temperature conditions, respectively:

$$T_1[y > 0, t = 0] = T_P \tag{5}$$

and

$$T_2[y < 0, t = 0] = T_0. \tag{6}$$

For many processes such as thermal spray and splat cooling, fast heat transfer may result in a significant melt undercooling during crystalline nucleation and growth and in solid overheating during melting [18]. For pure materials, there are then two unknown variables: the interface velocity and the temperature at the solid–liquid interface during melting and solidification. In addition to the energy balance condition, a kinetics relationship which correlates the interface velocity and the temperature must then also be introduced [11, 12]. A linear kinetics relationship can usually be a good approximation if the deviation of the interface temperature from the equilibrium melting temperature is moderate:

$$V_i = \mu_k(T_M - T_i) \tag{7}$$

where μ_k is the linear kinetics coefficient. It should be noted that although eqn (7) was derived from crystallization kinetics, it can also be applied as a first approximation to a melting process [19].

The energy balance conditions at the solid–liquid interface can be written for both deposit and substrate as

$$\rho_L L V_i = \lambda_S \frac{\partial T_S}{\partial y}\bigg|_i - \lambda_L \frac{\partial T_L}{\partial y}\bigg|_i \tag{8}$$

where L is the latent heat of fusion, V_i the interface velocity, and ρ_L the density. The superscripts S and L represent solid and liquid phase, respectively. The subscript i indicates that the gradients are evaluated at the solid–liquid interface.

The nucleation of a crystalline solid phase in the molten deposit is assumed to take place heterogeneously on the substrate surface at a nucleation temperature T_N lower than the equilibrium melting temperature T_{M1}. The subsequent deposit solidification may also include undercooling during the front advance. The melting of the substrate is assumed to take place when the substrate surface temperature reaches its equilibrium melting temperature, however, because of the smaller nucleation kinetics barrier for melting of a solid. Solid overheating is, however, introduced during the subsequent substrate melting because of the finite melting kinetics. Resolidification of the melted substrate material will begin when the heat flux from the solid–liquid interface into the solid substrate is larger than that from the melt into the interface. No nucleation model is necessary because the melt is already in contact with its own crystalline phase. Melt undercooling is, however, introduced during the course of resolidification based on the kinetics relationship quantified by eqn (7).

2.2. *Nondimensionalization of governing equations*

The equations listed above can be nondimensionalized with the deposit thickness b as the characteristic length, b^2/α_{L1} as the characteristic time, and $(T_{M2} - T_0)$ as the characteristic temperature difference. T_{M2} is the equilibrium melting temperature of the substrate and the subscript L1 indicates liquid (L) deposit (1). The following nondimensional distance Y, time τ and temperature θ can be defined:

$$Y = \frac{y}{b} \quad \tau = \frac{t\alpha_{L1}}{b^2} \quad \theta = \frac{T - T_0}{T_{M2} - T_0}. \tag{9}$$

All the equations listed above can then be nondimensionalized as follows:

for the liquid region in the deposit (L1)

$$\frac{\partial \theta_{L1}}{\partial \tau} = \frac{\partial^2 \theta_{L1}}{\partial Y^2} \tag{10}$$

for the solid region in the deposit (S1)

$$\frac{\partial \theta_{S1}}{\partial \tau} = \frac{\partial}{\partial Y}\left(\frac{\alpha_{S1}}{\alpha_{L1}} \frac{\partial \theta_{S1}}{\partial Y}\right) \tag{11}$$

for the liquid region in the substrate (L2)

$$\frac{\partial \theta_{L2}}{\partial \tau} = \frac{\partial}{\partial Y}\left(\frac{\alpha_{L2}}{\alpha_{L1}} \frac{\partial \theta_{L2}}{\partial Y}\right) \tag{12}$$

and for the solid region in the substrate (S2)

$$\frac{\partial \theta_{S2}}{\partial \tau} = \frac{\partial}{\partial Y}\left(\frac{\alpha_{S2}}{\alpha_{L1}} \frac{\partial \theta_{S2}}{\partial Y}\right). \tag{13}$$

The thermal balance at the interface between deposit and substrate becomes then

$$+ \frac{\lambda_{L1}}{\lambda_{L1}} \frac{\partial \theta_1}{\partial Y}\bigg|_{Y=0} = Bi(\theta_{1,0} - \theta_{2,0})$$

or

$$+ \frac{\lambda_{S1}}{\lambda_{L1}} \frac{\partial \theta_1}{\partial Y}\bigg|_{Y=0} = Bi(\theta_{1,0} - \theta_{2,0}) \tag{14}$$

for either the liquid or solid deposit phase in contact with the substrate, and

$$+ \frac{\lambda_{L2}}{\lambda_{L1}} \frac{\partial \theta_2}{\partial Y}\bigg|_{Y=0} = Bi(\theta_{1,0} - \theta_{2,0})$$

or

$$+ \frac{\lambda_{S2}}{\lambda_{L1}} \frac{\partial \theta_2}{\partial Y}\bigg|_{Y=0} = Bi(\theta_{1,0} - \theta_{2,0}) \tag{15}$$

for the substrate, where $Bi = hb/\lambda_{L1}$

The nondimensional energy balance conditions at the solid–liquid interface are

$$\frac{1}{Ste_1} V_{i1}^* = \frac{\lambda_{S1}}{\lambda_{L1}} \frac{\partial \theta_{S1}}{\partial Y}\bigg|_{i1} - \frac{\partial \theta_{L1}}{\partial Y}\bigg|_{i1} \tag{16}$$

in the deposit, and

$$\frac{C_{L2}}{C_{L1}} \frac{\rho_{L2}}{\rho_{L1}} \frac{1}{Ste_2} V_{i2}^* = \frac{\lambda_{S2}}{\lambda_{L1}} \frac{\partial \theta_{S2}}{\partial Y}\bigg|_{i2} - \frac{\lambda_{L2}}{\lambda_{L1}} \frac{\partial \theta_{L2}}{\partial Y}\bigg|_{i2} \tag{17}$$

in the substrate, where $V_i^* = bV_i/\alpha_{L1}$ (the nondimensional interface velocity).

The nondimensional linear kinetics relationships are:

$$V_{i1}^* = \mu_{k1}^*(\theta_{M1} - \theta_{i1}) \quad \text{and} \quad V_{i2}^* = \mu_{k2}^*(\theta_{M2} - \theta_{i2}) \tag{18}$$

where μ_k^* is the nondimensional kinetics coefficient defined as

$$\mu_k^* = \frac{b\mu_k(T_{M2} - T_0)}{\alpha_{L1}}. \tag{19}$$

Note that θ_{M1} and θ_{M2} are the nondimensional melting temperature of the deposit and substrate, respectively:

$$\theta_{M1} = \frac{T_{M1} - T_0}{T_{M2} - T_0} \quad \text{and} \quad \theta_{M2} = 1 \tag{20}$$

the latter by definition

The nondimensional initial conditions for the temperature in the deposit and substrate are then, respectively,

$$\theta_1[Y > 0, \tau = 0] = \theta_P \tag{21}$$

and

$$\theta_2[Y < 0, \tau = 0] = 0 \tag{22}$$

where θ_P is the nondimensional pouring temperature of the molten deposit

$$\theta_P = \frac{T_P - T_0}{T_{M2} - T_0}. \tag{23}$$

The nondimensional boundary conditions at the two end surfaces of the computational domain are

$$-\frac{\partial \theta_1}{\partial Y}\bigg|_{Y=1} = \frac{Q_s}{\lambda_1/\lambda_{L1}} \quad \text{and} \quad \theta_2[Y = -\infty, \tau] = 0 \tag{24}$$

with the dimensionless heat flux Q_s defined as

$$Q_s = \frac{q_s b}{\lambda_{L1}(T_{M2} - T_0)} \tag{25}$$

and λ_1/λ_{L1} being 1 before the deposit is solidified and $\lambda_{S1}/\lambda_{L1}$ after the deposit is solidified.

We assume that the deposit starts to solidify when the deposit bottom surface temperature ($T_{1,0}$) reaches the nucleation temperature (T_N), and that the substrate begins to melt when the substrate surface substrate ($T_{2,0}$) reaches the equilibrium melting temperature of the substrate material (T_{M2}). The corresponding nondimensional conditions are

$$\theta_{1,0} = \theta_N \quad \text{and} \quad \theta_{2,0} = 1. \tag{26}$$

It is now important to distinguish between several different situations:

(1) *Before substrate melting and without deposit solidification.* This is a pure heat conduction problem with a liquid deposit in contact with a solid substrate, and only eqns (10), (13)–(15), (21), (22) and (24) are needed. Five dimensionless parameters control the process:

$$Bi, \quad \theta_P, \quad Q_s \quad \frac{\alpha_{S2}}{\alpha_{L1}}, \quad \frac{\lambda_{S2}}{\lambda_{L1}}. \tag{27}$$

Among them, three dimensionless parameters—Bi, θ_P and Q_s—depend on the processing conditions, the other two being known for a specified material pair.

(2) *Before the substrate melts but with the deposit solidifying.* Eqns (10), (11), (13)–(16), (18), (21), (22) and (24) with 11 dimensionless parameters are needed to determine the substrate melting:

$$Bi, \quad \theta_P, \quad Q_s, \quad \theta_N, \quad \frac{\alpha_{S2}}{\alpha_{L1}}, \quad \frac{\alpha_{S1}}{\alpha_{L1}},$$

$$\frac{\lambda_{S2}}{\lambda_{L1}}, \quad \frac{\lambda_{S1}}{\lambda_{L1}}, \quad \mu_{k1}^*, \quad \theta_{M1}, \quad Ste_1. \tag{28}$$

Except for the first four, all these parameters are determined by the material properties of the deposit and substrate, and the controlling process parameters are therefore limited to Bi, θ_P, Q_s and θ_N for a given material pair.

(3) *Substrate melting and resolidification without deposit solidification.* The relevant governing eqns are (10), (12)–(15), (17), (18), (21), (22) and (24) which require again 11 dimensionless parameters:

$$Bi, \quad \theta_P, \quad Q_s, \quad \frac{\alpha_{S2}}{\alpha_{L1}}, \quad \frac{\alpha_{L2}}{\alpha_{L1}},$$

$$\frac{\lambda_{S2}}{\lambda_{L1}}, \quad \frac{\lambda_{L2}}{\lambda_{L1}}, \quad \frac{C_{L2}}{C_{L1}}, \quad \frac{\rho_{L2}}{\rho_{L1}}, \quad \mu_{k2}^*, \quad Ste_2. \tag{29}$$

(4) Finally, *substrate melting and resolidification with simultaneous deposit solidification.* All the equations are needed, namely (10)–(18), (21), (22) and (24); and the number of controlling dimensionless parameters increases to 16 (all the parameters listed above except for one of the property ratios which can be expressed as a function of the other ones). Here again, only four parameters (Bi, θ_P, Q_S and θ_N) involve the process parameters whereas all the other parameters are determined by the deposit and substrate material properties.

Clearly, the problem can become rather complex to solve if all the material properties are involved, but the use of this nondimensionalization approach shows that in all cases there are only two main process-related parameters controlling the substrate melting, and these involve only deposit thickness, interfacial thermal contact and initial temperature difference between deposit and substrate. This observation will

be the basis for the treatment and presentation of results shown below.

2.3. *Numerical solution method*

The mathematical problem described above is a moving boundaries problem with heat conduction in both deposit and substrate. An implicit control volume integral method with immobilization of the moving interface by coordinate transformation is used to solve this problem. This method is especially suitable for problems with a large difference in length scales between the solid and liquid regions. A brief description of the coordinate transformations technique is given here. A more detailed description of the generation of the nonuniform grid, the derivation of the difference equations, and the iteration scheme for the moving interface can be found elsewhere [20, 21].

In the deposit, the solid–liquid interface is 'immobilized' by transforming the original physical coordinates into computational coordinates through

$$\eta_1 = \frac{Y}{\varepsilon_1} \quad \text{and} \quad \xi_1 = \frac{Y-\varepsilon_1}{1-\varepsilon_1} \tag{30}$$

where Y is the nondimensional position in the original physical coordinates, ε_1 is the nondimensional solid–liquid interface elevation in the deposit, and η_1 and ξ_1 are the nondimensional space coordinates in the solid and liquid regions, respectively, in the computational plane. From eqn (30) we obtain transformation operators as follows:

in the solid region

$$\frac{\partial}{\partial Y} \Rightarrow \frac{1}{\varepsilon_1}\frac{\partial}{\partial \eta_1}, \quad \frac{\partial}{\partial \tau} \Rightarrow \frac{\partial}{\partial \tau} - \frac{\eta_1}{\varepsilon_1}\frac{\mathrm{d}\varepsilon_1}{\mathrm{d}\tau}\frac{\partial}{\partial \eta_1} \tag{31}$$

and in the liquid region

$$\frac{\partial}{\partial Y} \Rightarrow \frac{1}{1-\varepsilon_1}\frac{\partial}{\partial \xi_1}, \quad \frac{\partial}{\partial \tau} \Rightarrow \frac{\partial}{\partial \tau} + \left(\frac{\xi_1 - 1}{1-\varepsilon_1}\right)\frac{\mathrm{d}\varepsilon_1}{\mathrm{d}\tau}\frac{\partial}{\partial \xi_1}. \tag{32}$$

The following coordinate transformation relationships are used in the substrate:

$$\eta_2 = \frac{b_2 + Y}{b_2 + \varepsilon_2}, \quad \xi_2 = \frac{\varepsilon_2 - Y}{\varepsilon_2} \tag{33}$$

where ε_2 is the nondimensional solid–liquid interface distance in the substrate from the deposit–substrate interface, b_2 the nondimensional thickness of the computation domain in the substrate, η_2 is the transformed nondimensional space coordinate in the solid domain of the computational plane and ξ_2 is in the liquid domain. The corresponding coordinate transformation operators are then

$$\frac{\partial}{\partial Y} \Rightarrow \frac{1}{b_2 + \varepsilon_2}\frac{\partial}{\partial \eta_2}, \quad \frac{\partial}{\partial \tau} \Rightarrow \frac{\partial}{\partial \tau} - \left(\frac{\eta_2}{b_2 + \varepsilon_2}\right)\frac{\mathrm{d}\varepsilon_2}{\mathrm{d}\tau}\frac{\partial}{\partial \eta_2} \tag{34}$$

in the solid region of the substrate, and

$$\frac{\partial}{\partial Y} \Rightarrow \frac{1}{\varepsilon_2}\frac{\partial}{\partial \xi_2}, \quad \frac{\partial}{\partial \tau} \Rightarrow \frac{\partial}{\partial \tau} + \left(\frac{1-\xi_2}{\varepsilon_2}\right)\frac{\mathrm{d}\varepsilon_2}{\mathrm{d}\tau}\frac{\partial}{\partial \xi_2} \tag{35}$$

in the liquid region.

Introducing the transformation eqns (30)–(35) into the nondimensional governing equations, we can solve the latter using techniques developed previously [20, 21]. The finite difference equations for the nodal temperatures are obtained directly by the integration of the differential equations from t to $t+\Delta t$ over each control volume element using an implicit central difference scheme with a nonuniform grid. A zero width control volume is used for all interfaces and surfaces in order to calculate their temperatures. The difference equations for those temperatures are derived from balance conditions at the interfaces or boundary conditions at the surfaces. Finally, at each time step a TDMA algorithm is used to solve the difference equations in order to obtain temperature distributions in both deposit and substrate, including the solid–liquid interface temperature and all the surface temperatures. The solid–liquid interface advance is determined with the kinetics relation in eqn (7) based first on the calculated solid–liquid interface temperature at the previous time step. It is important to note, however, that the temperature field (including the interface temperature) and the front velocity are in fact coupled and that the equations must be solved simultaneously using an iteration technique until the temperature field has been determined in its entirety within the iteration convergence criterion. The numerical implementation was checked by comparing the results to those predicted by using very different numerical approaches such as interface tracking without coordinate transformation [12] and a modified version of the latent heat source method [11], in the simplified cases when these are applicable. Very good agreement was obtained.

Melting of the substrate is assumed to begin when its surface temperature reaches the equilibrium melting temperature of the given substrate material. By adjusting the input processing conditions such as the initial deposit and substrate temperatures and the interfacial heat transfer coefficient, one can determine the critical conditions under which substrate melting may take place. During substrate melting, the heat flux from the melt into the solid–liquid interface will be larger than that from the interface into the solid substrate. The differences between the two, however, decreases as the solid–liquid interface penetrates deeper and deeper into the substrate. At some point, the difference disappears and melting stops. After that, the heat flux from the interface into the solid becomes larger than that from the melt into the interface and the melt begins to resolidify. Once the interface velocity changes sign from negative to positive, resolidification starts and the solid–liquid interface location at that moment is assumed to be the maximum melting depth.

It should be pointed out that the model and the

corresponding numerical method proposed in this paper can be used for simulation of deposit cooling and substrate melting and resolidification problems with or without undercooling and overheating. In the present paper we focus on the melting and resolidification of materials with relatively low melting temperature for which the substrate melting takes place before deposit solidification. Processes where the deposit solidifies before or at the same time as the substrate melts will be discussed elsewhere.

3. COMPUTATIONAL RESULTS AND DISCUSSIONS

As shown in our nondimensional analysis, the phenomenon of substrate melting and solidification after impact by a molten layer is a complex problem controlled by many dimensionless parameters. In this article we limit ourselves to the case of a substrate which melts and resolidifies before the deposit solidifies [cases (1) and (3) above], which would happen for a deposit of relatively low melting point material with high superheat, such as in spray casting and microcasting processes. In this case, the nucleation temperature of the deposit does not play a role in the substrate melting, and for a given deposit and substrate materials the only controlling parameters related directly to the process configuration and conditions are Bi, θ_P and Q_s. We have conducted some calculations for several common materials, such as copper, aluminum, nickel and steel. (The physical properties used in the calculations are given in Table 1. These are assumed to remain independent of temperature, although being different in the solid and liquid phases.)

In all the following calculations, it was assumed that the heat flux in or out of the deposit top surface is negligible, i.e. $Q_s = 0$. This assumption is justified here because the main concern of this study is the interaction between the deposit and the substrate, which is a local phenomenon that takes place far away from the splat top surface. Additionally, in most cases the heat transfer rate between the deposit top surface and the environment is much smaller than that between the deposit and the substrate, and neglecting the top surface heat flux will have little effect on the model predictions of substrate melting and resolidification. This is true for most of the processes we are interested in here such as microcasting, splat cooling and melt-spinning. Even for plasma thermal spraying where the deposit is heated by a high temperature plasma, the heat transfer into the deposit is still much smaller than the heat transferred from the deposit into the substrate, because of the greatly enhanced thermal contact between the deposit and substrate due to high droplet impact velocity. In any case the numerical model developed here can readily accommodate the introduction of an additional heat flux at the top surface of the deposit if warranted.

3.1. *Operational map: critical conditions for substrate melting*

The most basic question one may be faced with when dealing with this type of problem is whether the substrate will melt for given process parameters or, conversely, what process conditions will result in melting for a given set of material and geometry. This information is provided in nondimensional form in operational maps we have developed for a number of material combinations.

Figure 2 shows an operational map containing information about the process conditions leading to substrate melting. Figure 2 gives the necessary nondimensional pouring superheat θ_P as a function of Bi to reach the onset of substrate melting for five different materials pairs. The curves divide the process conditions plane into two regions. Below the curve, no melting of the substrate will occur, whereas above the curve substrate melting will indeed take place. This map was generated through systematic variations of the process parameters and analysis of the corresponding temperature profiles predicted by the model which reveals readily whether substrate melting takes place or not for the given process parameters.

Table 1. Physical property values used in the calculations [24, 25]

Parameter	Units	Al	Cu	Ni†	Steel
T_m	K	933.6	1356	1728	1788
L	J kg^{-1}	3.97×10^5	2.0×10^5	2.92×10^5	2.72×10^5
λ_L	W m-K^{-1}	105	170	43	26
λ_S	W m-K^{-1}	210	244	74	28
C_{PL}	J kg-K^{-1}	1080	495	620	866.67
C_{PS}	J kg-K^{-1}	1180	473	595	690.82
ρ_L	kg m^{-3}	2390	8000	7900	7700
ρ_S	kg m^{-3}	2550	8900	8900	7850
α_L	m^2 s^{-1}	4.1×10^{-5}	4.3×10^{-5}	0.9×10^{-5}	0.39×10^{-5}
α_S	m^2 s^{-1}	7.0×10^{-5}	5.8×10^{-5}	1.4×10^{-5}	0.52×10^{-5}
$\Delta S_m/R$	—	1.35	1.15	1.19	0.9
μ_k	m s-K^{-1}	1.74	0.94	0.85	0.01

† Thermal conductivity data from ref. [25].

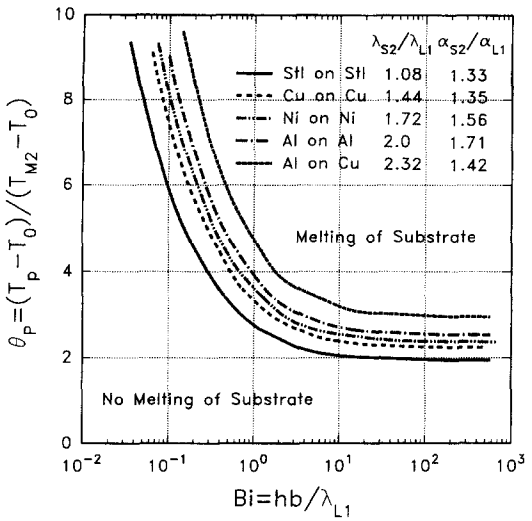

Fig. 2. Operational map for a substrate impacted by a superheated molten metal deposit. The curves show the onset of substrate melting.

(It should be noted that the high values of θ_P could indeed easily be reached for high initial substrate temperature.) As one expects, it is seen that for a lower value for *Bi* (i.e. a poor thermal contact deposit and substrate or a thin deposit) a higher value of θ_P (i.e. a high deposit superheat or a high substrate initial temperature) is needed to make substrate melting possible. Conversely, for high *Bi*, the critical θ_P decreases. When *Bi* is small, less than 10, say, a relatively large decrease in the necessary θ_P will result from a small increase in *Bi*, but when *Bi* is larger, a further increase in *Bi* will lead to little variation in the critical θ_P. This small sensitivity on *Bi* can be understood considering that if the thermal contact between deposit and substrate is very good, the controlling heat transfer resistance will be the conduction resistance in the deposit or in the substrate. There is, therefore, a limiting value of θ_P (e.g. $\theta_P \approx 3$ for Al deposited on a Cu substrate) below which no substrate melting is possible even for very thick deposit or very good contact.

For a given *Bi*, the θ_P necessary to induce melting depends on the deposit and substrate material properties, through the two dimensionless parameters $\lambda_{S2}/\lambda_{L1}$ and α_{S2}/α_{L1}. Interestingly, the ratio of thermal conductivities $\lambda_{S2}/\lambda_{L1}$ is a better relative indicator of the ease of substrate melting for various material pairs than α_{S2}/α_{L1}, despite the unsteady nature of the problem. Of course, the larger the ratio $\lambda_{S2}/\lambda_{L1}$ is, the more difficult it is to have the substrate melt, because a large substrate thermal conductivity will carry heat away deep into the substrate and because a small deposit conductivity will be ineffective at carrying heat to the substrate surface, both effects resulting in a lower substrate surface temperature and therefore also lower likelihood of it exceeding the substrate melting temperature.

3.2. *Operational map: maximum melting depth in the substrate*

After one ascertains that the substrate will melt, it is important to determine by how much, either to determine whether bonding between layers will be sufficient, or conversely whether mold or casting wheel will be significantly damaged. Here again, we attempted to present the information in readily usable nondimensional terms.

As discussed above, for a given materials pair, and as long as deposit solidification takes place after substrate melting and resolidification, only two main parameters related to the process conditions (*Bi* and θ_P) control the substrate melting. Taking *Bi* as the independent parameter, another type of operational map can be generated by plotting the dimensionless maximum melting depth, d_{max}/b, as a function of θ_P for a number of *Bi* values, as shown in Fig. 3(a)–(c), for Cu on Cu, Al on Al, and steel on steel, respectively. These values were obtained from interface tracking results obtained in a parametric study. In Fig. 3(a)–(c), the thermal contact condition between the deposit and the substrate is assumed to remain the same before and after the substrate is melted. In the next section, however, it will be shown that variations in h due to the phase change could result in large variations in the process. As we could also see in Fig. 2 for any *Bi* value, a critical θ_P must be exceeded for melting to take place, and the higher the θ_P beyond that minimum, the more the substrate will melt. It can indeed be seen in Fig. 3 that a small increase in θ_P beyond the minimum needed for substrate melting will result in a large relative increase in the maximum melting depth in the substrate. For large θ_P, the melted depth is no longer increasing so readily with an increase in θ_P and it becomes proportionally more costly (in θ_P terms) to melt more of the substrate. This takes place for $d_{max}/b > 0.01$ or so.

Increasing the *Bi* decreases the θ_P needed to start melting, as already pointed out above, but the general trends of the relationship between θ_P and d_{max} are similar. The *Bi* number also has a strong effect on the maximum melting depth. At a given θ_P if the *Bi* is large enough to result in substrate melting, we see that the melted depth will first increase fast with increasing *Bi*, but then less so as the *Bi* becomes large. Again, this is because the main resistance to heat transfer will be in the deposit or substrate for the case of good thermal contact or thick deposit (i.e. high *Bi*), and the thermal contact resistance will no longer be the dominant factor.

The material properties do, of course, affect greatly the extent of substrate melting and resolidification, and in order to illustrate this effect we show some results for Al on Al ($\lambda_{S2}/\lambda_{L1} = 2.0$) and steel on steel ($\lambda_{S2}/\lambda_{L1} = 1.08$) in Fig. 3(b) and (c). The overall variations in d_{max}/b with θ_P and the effect of *Bi* are similar in all cases. The melting depth increases faster with increasing θ_P for steel than for Al, however, because the ratio of substrate to deposit conductivity is

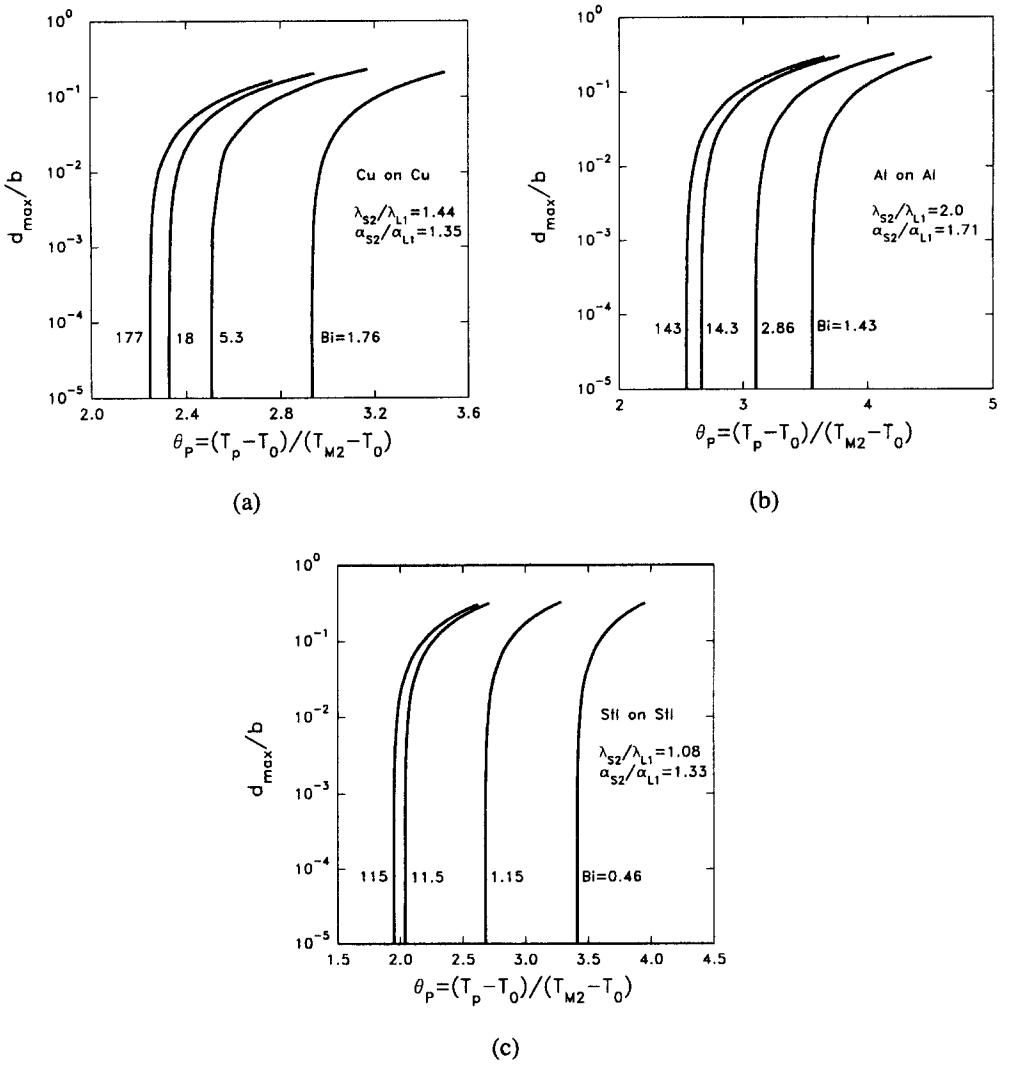

Fig. 3. Maximum melting depth in a substrate impacted by a molten metal deposit under various process conditions for (a) Cu on Cu, (b) Al on Al, and (c) steel on steel. (Thermal contact between deposit and substrate assumed constant.)

smaller, meaning the heat is more readily brought to the substrate surface from the deposit and less readily removed to the substrate underneath.

3.3. *Effect of interfacial heat transfer on the maximum melting depth of the substrate*

The results shown in Fig. 3(a)–(c) were obtained under the assumption that the thermal contact between the deposit and the substrate does not change as the substrate melts. However, this assumption may not be valid in some cases. Indeed, after the substrate melts, the initial liquid (deposit)–solid (substrate) contact becomes a liquid–liquid contact. It is believed that the nonperfect thermal contact between the deposit and the solid substrate is mainly due to the microscopic roughness of the solid surface. When the substrate melts, those corresponding micro-roughnesses disappear, and a better contact between the liquid deposit and the liquid substrate surface would result, although an oxide film and other surface contaminants or gas entrapment might still be present. It is, therefore, expected that the interfacial heat transfer coefficient h would increase as the substrate melts, which would in turn have a large effect on the substrate melting and resolidification. We have indeed measured dramatic changes in h for splat solidification processes. For example, we saw a two- to eight-fold increase in the interfacial heat transfer coefficient in some of our splat cooling experiments for a molten copper splat solidifying on metallic substrates, and also a dramatic decrease in h by a factor of up to 50 after the splat is solidified [16, 17, 22].

This effect is quantified in Fig. 4(a)–(c) which show the dimensionless maximum melting depth d_{max}/b as a function of dimensionless initial temperature θ_P for three deposit–substrate materials: Cu on Cu, Al on Al and steel on steel. The curves in those figures represent a different variation of Bi with time. For sim-

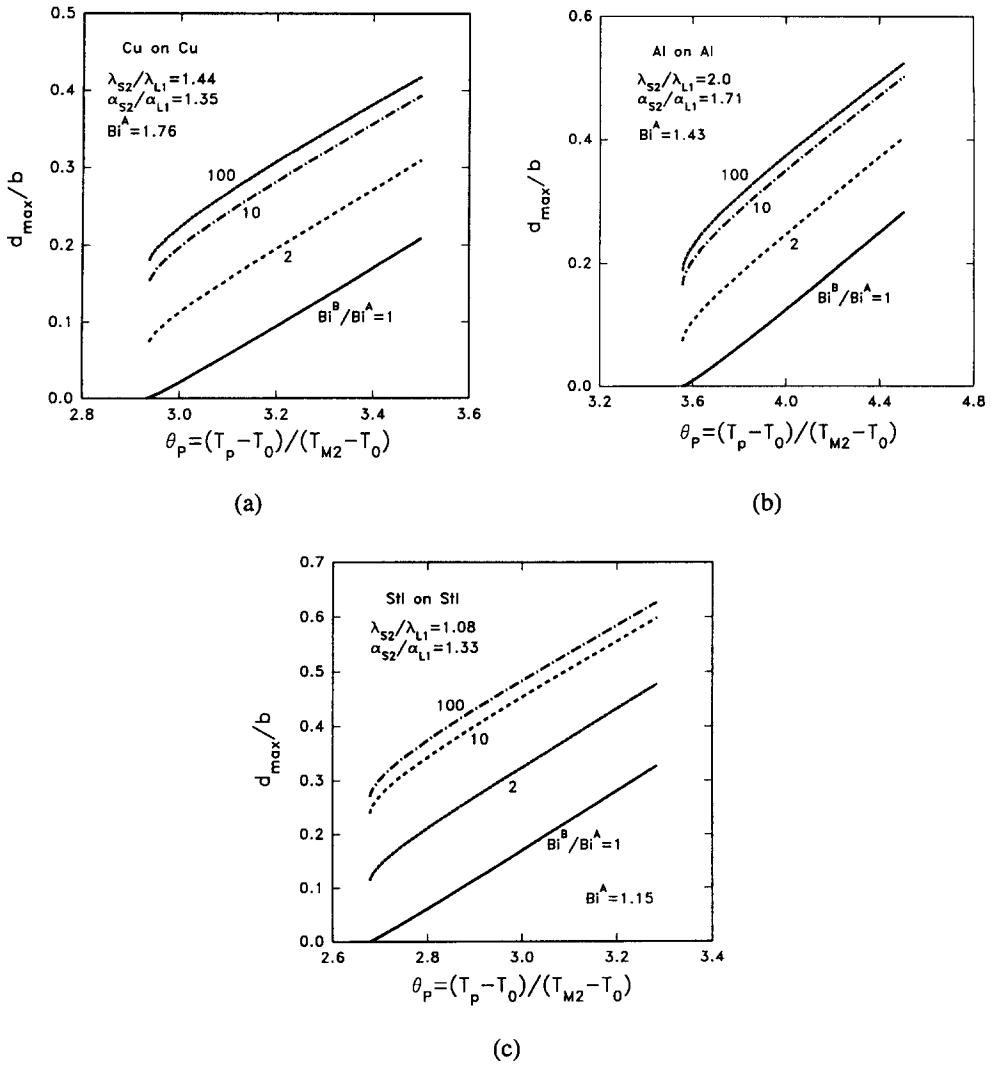

Fig. 4. Maximum melting depth in a substrate impacted by a molten metal deposit for various levels of increase in thermal contact between deposit and substrate upon substrate melting. (a) Cu on Cu, (b) Al on Al, and (c) steel on steel.

plicity, a step increase in *Bi* is assumed to take place when the substrate begins to melt. For example, in Fig. 4(a) for Cu on Cu, the curves correspond to a *Bi* increasing by a factor of 2, 10 and 100 upon melting, and the variation of d_{max}/b with θ_P is similar in all cases. We see a large increase in predicted melting depth if one accounts for even a relatively small (a factor of 2, say) increase in h upon melting. This effect tapers off if the h increases very much, again because the limiting factor becomes then conduction in the deposit and substrate. For example, the difference between the cases where h increases by a factor of 10 or 100 is relatively small, and will become insignificant beyond that. Clearly though, these results suggest that it is necessary to account for even a small increase in h if one wants to predict the melting depth correctly. Similar trends and relative increases hold for the other materials pairs quantified.

3.4. *Substrate melting and resolidification characteristics*

The characteristics of the melting and resolidification of a substrate impacted by a molten deposit may be better understood by looking at the displacement and velocity of the solid–liquid interface. Figure 5 shows the solid–liquid interface location as a function of time for a copper deposit on a copper substrate and for four values of θ_P. (Here we are assuming again a constant *Bi* during the entire process.) We see that after a delay necessary to heat the substrate, the latter starts to melt and the solid–liquid interface moves deeper into the substrate. The higher the θ_P, the earlier the melting starts, the faster the solid–liquid interface moves, and the deeper the substrate will melt. After the maximum melting depth is reached, the melt will resolidify back to the substrate surface. The larger the θ_P, e.g. the higher the initial

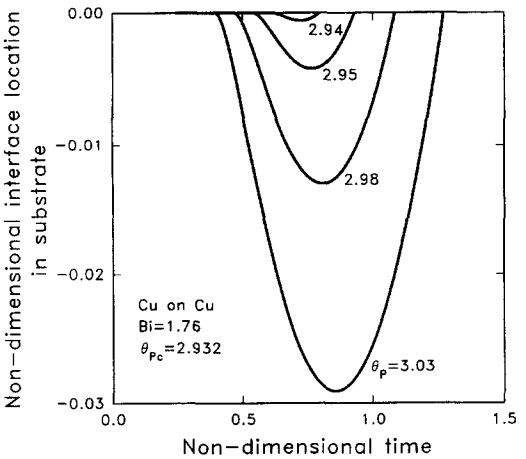

Fig. 5. Interface location as a function of time during melting and resolidification of a Cu substrate impacted by a molten Cu deposit ($Bi^A = Bi^B$).

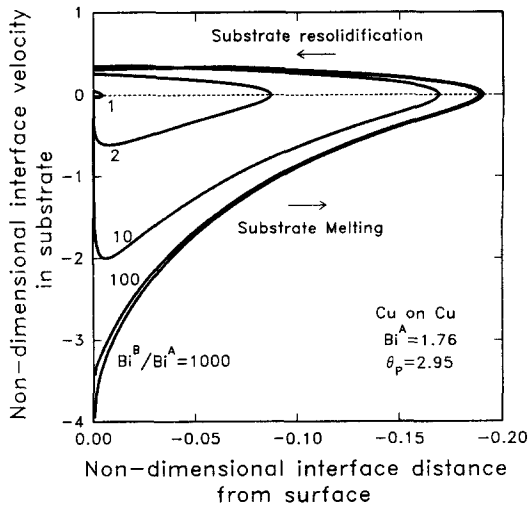

Fig. 7. Interface velocity during melting and resolidification of a Cu substrate impacted by a molten Cu deposit as a function of the interface depth for various levels of increase in deposit–substrate thermal contact upon substrate melting.

melt superheat, the longer it will take to complete the whole process.

The corresponding interface velocity (i.e. the rate of melting and resolidification) as a function of the interface depth is given in Fig. 6 for the same conditions as those of Fig. 5. (In this graph, the negative values of V_i correspond to melting and the positive values to resolidification.) In all cases the melting rate increases fast at the beginning when the substrate starts to melt, reaches a maximum and then slows down until the end of the melting process. Resolidification of the melt starts then slowly and speeds up to the end of resolidification when the interface reaches back to the substrate surface. The calculations take into account the departures from equilibrium at the solid–liquid interface, and we computed the overheating during substrate melting and the undercooling during substrate resolidification. These are proportional to the interface velocity since the linear kinetics model is used.

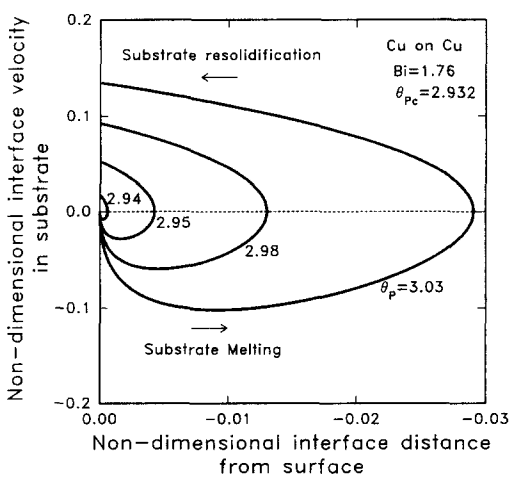

Fig. 6. Interface velocity as a function of interface depth during melting and resolidification of a Cu substrate impacted by a molten Cu deposit ($Bi^A = Bi^B$).

Here again, an increase in Bi due to a better thermal contact between the deposit and the substrate as the substrate melts will have a strong effect on the substrate melting and resolidification. This is quantified in Fig. 7, which shows the solid–liquid interface velocity during melting and resolidification as a function of the interface location for increases in Bi upon melting ranging from 2 to 1000. When the thermal contact increases, the melting rate increases sharply soon after melting and decreases slowly as the solid–liquid interface moves into the substrate. This results from the improved heat transfer between the deposit and substrate. For moderate increases in Bi, we can still see a maximum in melting rate, but if h increases by a factor of 100 or more, the melting rate is very large immediately after melting and decreases uniformly after that. The higher the improvement in h, the higher the melting rate and the greater the penetration depth, but the saturation effect is clearly seen here too for very large Bi ratios. The effect on the resolidification rate is not as dramatic as on the melting rate, because the heat content of the deposit is reduced by then and the thermal contact resistance is no longer a major factor.

4. CONCLUSIONS AND SUMMARY

A numerical model was developed to calculate substrate melting and resolidification when a substrate is impacted by a molten deposit. The model includes heat transfer in both deposit and substrate as well as departures from equilibrium at the solid–liquid interfaces, and variations with time of the thermal contact at the deposit–substrate interface. This problem is solved by using an implicit control volume method with interface tracking and solid–liquid interface immobilization by coordinate transformation.

The calculations were conducted in nondimensional

terms in order to obtain results of general applicability. We have generated nondimensional operational maps that allow us to predict readily whether substrate melting will take place or not, and by how much. For a given materials pair, the independent process parameters required are the Biot number and the nondimensional superheat if the substrate melts before the deposit solidifies. Parametric studies were conducted to quantify the effect of material properties and process parameters. We also showed that even relatively small increases in thermal contact between deposit and substrate as the substrate melts would result in large change in melted depth and melting rate, but that this effect tapers off for large increases in thermal contact. The melting and resolidification velocities were also quantified for various process conditions. The results can be explained using a combination of unsteady thermal considerations in the deposit and substrate.

Similar parametric studies were conducted for a number of material combinations. We believe that these results and in particular the nondimensional operational maps should be very useful for the process designer or user to find out readily how much substrate melting would result from given process parameters, or conversely would enable the use to tailor the process conditions to achieve an optimum melting depth or to avoid melting, as desired.

Acknowledgement—The authors would like to acknowledge gratefully the financial support of the U.S. National Science Foundation (grant number MSS-8957733 to E.F.M.).

REFERENCES

1. McPherson, R., The relationship between the mechanism of formation, microstructure and properties of plasma-sprayed coatings. *Thin Solid Film*, 1981, **83,** 297–310.
2. Zaat, J. H., A quarter of a century of plasma spraying. *Annual Review of Material Science*, 1983, **13,** 9–42.
3. Steffens, H.-D., Wielage, B. and Drozak, J., Interface phenomena and bonding mechanism of thermally-sprayed metal and ceramic composites. *Surface Coatings Technology*, 1991, **45,** 290–308.
4. Amon, C. H., Merz, R., Prinz, F. B. and Schmaltz, K. S., Thermal modeling and experimental testing of MD spray shape deposition processes. In *Heat Transfer* 1994, *Proceedings of Tenth International Heat Transfer Conference*, Vol. 7, pp. 321–324, ed. G. F. Hewitt, IChemE Publishing, Brighton, 1994.
5. Amon, C. H., Schmaltz, K. S., Merz, R. and Prinz, F. B., Numerical and experimental investigation of interface bonding via substrate remelting of an impinging molten metal droplet. *Journal of Heat Transfer*, 1996, **118,** 164–172.
6. Harmsworth, P. D. and Stevens, R., Microstructure of zirconia-yttria plasma-sprayed thermal barrier coatings. *Journal of Material Science*, 1992, **27,** 616–624.
7. Prinz, F. B., Weiss, L. E., Amon, C. H. and Beuth, J. L., Processing, thermal and mechanical issues in shape deposition manufacturing. In *Solid Freeform Fabrication Proceedings*, September, 1995, pp. 118–129.
8. Liu, H., Lavernia, E. J. and Rangel, R. H., Numerical simulation of substrate impact and freezing of droplets in plasma spray processes. *Journal of Physics D. Applied Physics*, 1993, **26,** 1900–1908.
9. Trapaga, G., Matthys, E. F., Valencia, J. J. and Szekely, J., Fluid flow, heat transfer and solidification of molten droplets impinging on substrates: comparison of numerical and experimental results. *Metallurgical and Materials Transactions B*, 1992, **23B,** 701–718.
10. Fukai, J., Zhao, A., Poulikakos, D., Megaridis, C. M. and Miyatake, O., Modeling of the deformation of a liquid droplet impinging upon a flat surface. *Physics of Fluids A*, 1993, **5,** 2588–2599.
11. Clyne, T., Numerical treatment of rapid solidification. *Metallurgical and Materials Transactions B*, 1984, **15B,** 369–381.
12. Wang, G. X. and Matthys, E. F., Numerical modeling of phase change and heat transfer during rapid solidification processes: use of control volume integral with element subdivision. *International Journal of Heat and Mass Transfer*, 1992, **35,** 141–153.
13. Kuijpers, T. W. and Zaat, J. H., Influence of oxygen and cooling rate on the microstructure and microhardness of plasma-sprayed molybdenum. *Metals Technology*, 1974, **1,** 142–150.
14. Sobolev, V. V., Guilemany, J. M. and Calero, J. A., Substrate-coating thermal interaction during high velocity oxyfuel spraying part I—heat transfer processes. *Material Science Technology*, 1995, **11,** 810–819.
15. Kang, B., Waldvogel, J. and Poulikakos, D., Remelting phenomena in the process of splat solidification. *Journal of Material Science*, 1995, **30,** 4912–4925.
16. Wang, G.-X. and Matthys, E. F., Experimental investigation of interfacial thermal resistance for molten metal solidification on a substrate. *Journal of Heat Transfer*, 1996, **118,** 157–163.
17. Wang, G.-X. and Matthys, E. F., On the heat transfer at the interface between a solidifying metal and a solid substrate. In *Melt-Spinning, Strip Casting, and Slab Casting*, ed. E. F. Matthys and W. G. Truckner. TMS, Warrendale, PA, 1996, pp. 205–236.
18. Wang, G.-X. and Matthys, E. F., Modeling of non-equilibrium surface melting and resolidification for pure metals and binary alloys. *Journal of Heat Transfer*, 1996, **118,** 944–951.
19. MacDonald, C. A., Malvexixi, A. M. and Spaepen, F., Picosecond time-resolved measurements of crystallization in noble metals. *Journal of Applied Physics*, 1989, **65,** 129–136.
20. Wang, G.-X. and Matthys, E. F., Modeling of rapid planar solidification of a binary alloy. In *Heat and Mass Transfer in Materials Processing and Manufacturing*, ed. D. Zumbrunnen *et al.*, HTD-Vol. 261. ASME, New York, 1993, pp. 35–44.
21. Wang, G.-X. Prasad, V. and Matthys, E. F., An interface tracking numerical method for rapid planar solidification of binary alloys with application to microsegregation. *Journal of Materials Science and Engineering A*, 1997, **A225,** 17–58.
22. Wang, G.-X. and Matthys, E. F., Interfacial thermal contact during rapid solidification on a substrate. In *Heat Transfer* 1994, *Proceedings of Tenth International Heat Transfer Conference*, Vol. 4, ed. G. F., Hewitt, IChemE Publishing, Brighton, 1994, pp. 169–174.
23. Brandes, E. A., *Smithells Metals Reference Book*, 6th edn. Butterworths, London, 1983.
24. Iida, T. and Guthrie, R. I. L., *The Physical Properties of Liquid Metals*. Clarendon, Oxford, 1988, pp. 10–108.
25. Hsu, S. C., Chakravorty, S. and Mehrabian, R., Rapid melting and solidification of a surface layer. *Metallurgical and Materials Transactions B*, 1978, **9B,** 221–229.